THE JOURNAL OF PHYSICAL CHEMISTRY B

Article

pubs.acs.org/JPCB

Hydrolysis of DFP and the Nerve Agent (*S*)-Sarin by DFPase Proceeds along Two Different Reaction Pathways: Implications for Engineering Bioscavengers

Troy Wymore,*[,†,∥] Martin J. Field,[‡] Paul Langan,[§] Jeremy C. Smith,[†,∥] and Jerry M. Parks*[,†]

[†]UT/ORNL Center for Molecular Biophysics, Biosciences Division, Oak Ridge National Laboratory, Oak Ridge, Tennessee 37831-6309, United States

[‡]Institut de Biologie Structurale "Jean-Pierre Ebel", 41 rue Jules Horowitz, 38027 Grenoble Cedex 1, France

[§]Center for Structural and Molecular Biology, Biology and Soft Matter Division, Oak Ridge National Laboratory, Oak Ridge, Tennessee 37831-6309, United States

[∥]Department of Biochemistry and Cellular and Molecular Biology, University of Tennessee, Knoxville, Tennessee 37996, United States

Supporting Information

ABSTRACT: Organophosphorus (OP) nerve agents such as (*S*)-sarin are among the most highly toxic compounds that have been synthesized. Engineering enzymes that catalyze the hydrolysis of nerve agents ("bioscavengers") is an emerging prophylactic approach to diminish their toxic effects. Although its native function is not known, diisopropyl fluorophosphatase (DFPase) from *Loligo vulgaris* catalyzes the hydrolysis of OP compounds. Here, we investigate the mechanisms of diisopropylfluorophosphate (DFP) and (*S*)-sarin hydrolysis by DFPase with quantum mechanical/molecular mechanical umbrella sampling simulations. We find that the mechanism for hydrolysis of DFP involves nucleophilic attack by Asp229 on phosphorus to form a pentavalent intermediate. P−F bond dissociation then yields a phosphoacyl enzyme intermediate in the rate-limiting step. The simulations suggest that a water molecule, coordinated to the catalytic Ca^{2+}, donates a proton to Asp121 and then attacks the tetrahedral phosphoacyl intermediate to liberate the diisopropylphosphate product. In contrast, the calculated free energy barrier for hydrolysis of (*S*)-sarin by the same mechanism is highly unfavorable, primarily because of the instability of the pentavalent phosphoenzyme species. Instead, simulations suggest that hydrolysis of (*S*)-sarin proceeds by a mechanism in which Asp229 could activate an intervening water molecule for nucleophilic attack on the substrate. These findings may lead to improved strategies for engineering DFPase and related six-bladed β-propeller folds for more efficient degradation of OP compounds.

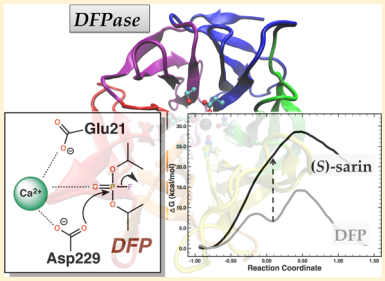

INTRODUCTION

Organophosphorus (OP) compounds are used as pesticides, insecticides, and chemical nerve agents such as sarin (GB), tabun (GA), soman (GD), and VX (Figure 1). OP compounds inhibit acetylcholinesterase (AChE) by forming a covalent adduct with an active site serine residue, leading to over-stimulation of the nervous system and subsequently to respiratory failure and death. Chemical rescue of AChE can be accomplished by administering oximes[1,2] or other "reactivators",[3] but this approach has shown only limited efficacy. Moreover, covalent adducts of AChE undergo spontaneous dealkylation, or "aging", which renders adduct formation irreversible.[4,5] Therefore, there is great interest in developing new approaches for protection against OP compounds.[6] An important detoxification strategy involves using enzymes as catalytic bioscavengers to degrade OP compounds before they can reach AChE.[7,8]

Many enzymes are known to display low-level hydrolase activity toward OP compounds and several have been investigated as potential catalytic bioscavengers.[8] Substantial effort has been directed toward improving the catalytic activity and enantioselectivity of bioscavengers toward OP nerve agents through rational design and directed evolution approaches. Notable examples include organophosphorus hydrolase (OPH), also called phosphotriesterase (PTE),[9,10,11] from the soil bacterium *Brevundimonas diminuta*, human serum paraoxonase (PON1),[12,13] and diisopropyl fluorophosphatase (DFPase) from the European squid, *Loligo vulgaris*.[14,15] Wild-type PON1 and DFPase exhibit a preference for the less toxic (*R*)-enantiomers of G-type nerve agents.

To design improved variants of OP hydrolases, it is beneficial to understand the biochemical mechanisms[11] of these enzymes with various substrates. Several aspects of the mechanism of DFP hydrolysis by DFPase have been determined experimentally. For example, the pH−rate profile for the reaction revealed that a protein residue with an apparent pK_a of ∼6.8

Received: October 21, 2013
Revised: April 10, 2014
Published: April 10, 2014

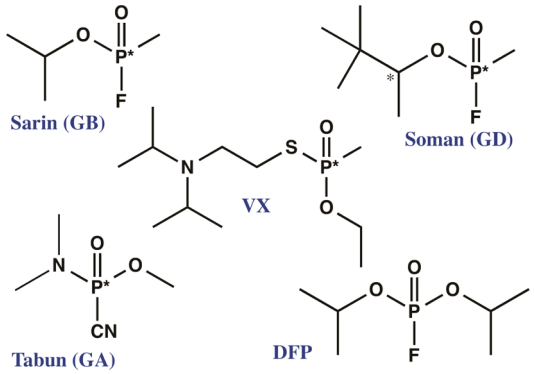

Figure 1. Structural diagrams of selected nerve agents. An asterisk denotes a chiral center.

must be deprotonated for maximal catalytic activity.[16] The experimentally measured k_{cat} for the hydrolysis of DFP by wild-type DFPase is 211 ± 9 s^{-1}.[15] On the basis of mutagenesis studies, active site residue His287 was shown not to play a major role in catalysis and is not essential for activity.[17] Single- and multiple-turnover reactions in $H_2{}^{18}O$ demonstrated that a carboxylate oxygen from Asp229 is incorporated into the DFP hydrolysis product, diisopropylphosphate,[14] establishing that a covalent phosphoenzyme intermediate is formed between Asp229 and DFP (Figure 2). A water molecule is then presumed to attack the phosphoacyl enzyme intermediate (Cγ of Asp229) to liberate diisopropylphosphate and to complete the catalytic cycle. Brønsted analysis of PON1 with analogues of paraoxon revealed a β_{LG} value of −1.6 for leaving groups with pK_a's > 7, suggesting that the transition state is very late and leaving group dissociation is fully rate limiting.[18]

Several high-resolution X-ray crystal structures[14,19,20] and one joint X-ray/neutron (X/N) diffraction structure of DFPase[21] provide insight into the possible binding modes of OP substrates and protonation states of key residues and also enable simulation of substrate binding and catalysis. DFPase exhibits many structural similarities to PON1. Although the amino acid sequences of DFPase and PON1 display significant divergence,[22] each has a six-bladed β-propeller fold with two Ca^{2+} metal ions: one required for catalysis and the other, located in the central water tunnel, providing structural integrity.[21,23,24] The first β-strand of each blade contributes at least one residue to the active site (Figure 3), although they are

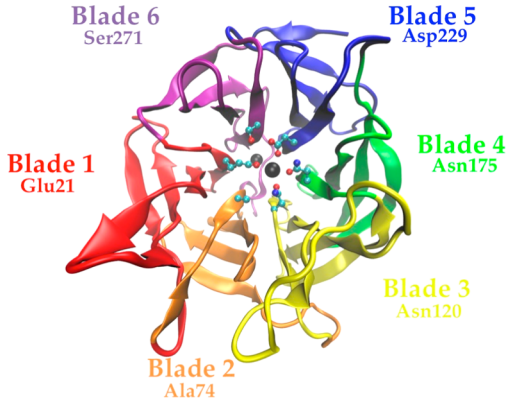

Figure 3. Structural depiction of DFPase showing each blade of the six-bladed β-propeller fold with the active site residue from each blade shown in the CPK representation. Black spheres represent the catalytic (foreground) and structural (background) Ca^{2+} ions.

not all coordinated to the catalytic Ca^{2+}. Notable examples are Ala74/His115 and Ser271/Thr332 (DFPase/PON1). The X/N structure of DFPase crystallized at pH 6.5 revealed that all active site residues are in their canonical protonation states and that two neutral water molecules, as opposed to hydroxides, are coordinated to the catalytic Ca^{2+}. Thus, modeling the nucleophilic attack by Asp229 on OP compounds does not require examination of any Asp229 activation steps by Ser271, although this step has also been proposed as part of the mechanism for DFPase.[25] A recent report of a high-resolution X-ray structure of DFPase determined at 0.85 Å resolution suggests that a third water molecule, bound to the catalytic Ca^{2+}, shares a proton with Asp229.[26] The authors proposed that this water molecule is partially activated and may play a role in enzyme regeneration.

Various aspects of DFPase-catalyzed OP hydrolysis mechanisms remain to be determined conclusively. For example, it is not known whether nucleophilic attack on the substrate involves a one-step A_nD_n-like transition or proceeds through a trigonal bipyramidal/pentavalent intermediate (A_n + D_n).[27,28] Moreover, the roles of intermolecular interactions in the active site that facilitate elimination of the fluoride leaving group have not been investigated. Another question concerns how a water molecule is activated for attack on the tetrahedral phosphoacyl enzyme intermediate. It is also not known whether the

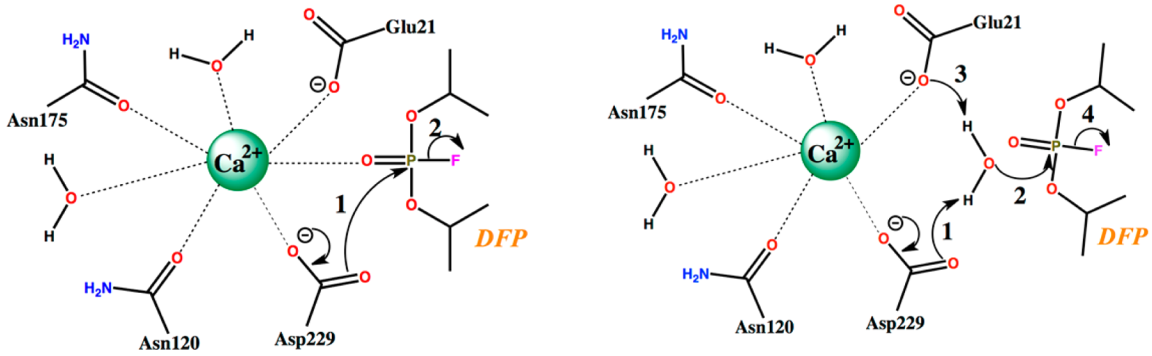

Figure 2. (Left) Proposed mechanism for phosphoenzyme intermediate formation involving Asp229 as the nucleophile. (i) Asp229 attacks the phosphorus center of DFP to form a pentavalent intermediate and (ii) the P−F bond dissociates to form a tetrahedral phosphoenzyme intermediate. Hydrolysis of the phosphoenzyme intermediate is not shown. (Right) Proposed mechanism for hydrolysis involving an activated water as the nucleophile. (i) Asp229 abstracts a proton from a water molecule either stepwise or in concert as (ii) water attacks the phosphorus center, (iii) Glu21 abstracts a proton either stepwise or in concert as (4) water forms a bond with phosphorus, and (iv) the P−F bond dissociates.

dx.doi.org/10.1021/jp410422c | J. Phys. Chem. B 2014, 118, 4479−4489

hydrolysis of all OP compounds share the same mechanism. Answers to these questions would be useful in interpreting DFPase and PON1 engineering studies and may help to guide rational enzyme design efforts.

Here, we perform quantum mechanical/molecular mechanical[29−31] (QM/MM) umbrella sampling simulations with density functional theory to investigate and compare the mechanisms of DFP and (*S*)-sarin hydrolysis by DFPase. We then analyze the underlying energetics of nucleophilic attack by a carboxylate nucleophile on both substrates and characterize important differences between them. Lastly, we discuss the implications of our findings for designing improved nerve agent bioscavengers.

METHODS

System Preparation. Although the substrates diisopropyl fluorophosphate (DFP) and isopropyl methylphosphonofluoridate (sarin) were included in the QM subsystem during the QM/MM simulations, we performed initial system equilibration steps with classical MM MD. Thus, we generated CHARMM force field parameters for DFP and sarin by analogy to existing parameters and made appropriate modifications. The ParamChem web server (www.paramchem.org)[32,33] was used to generate initial topology and parameter sets for diisopropylphosphate and isopropyl methylphosphonate, which were then modified for use with DFP and sarin. Equilibrium bond lengths and angles were obtained from B3LYP/6-31+G(d) geometry optimizations, and charges were obtained from Mulliken population analysis with ORCA.[34] Parameter sets for DFP and sarin are provided in the Supporting Information.

Atomic coordinates for the simulations were obtained from the 1.73 Å resolution X-ray cocrystal structure of DFPase from *L. vulgaris* with the DFP analogue dicyclopentyl phosphoramidate (DcPPA) (PDB entry 2GVV).[15] Protonation states were assigned on the basis of a joint X-ray/neutron diffraction structure of *apo* DFPase (PDB entry 3BYC),[21] which revealed that all protein side chains are in their standard pH 7 ionization states. Two systems were simulated: one with DFP as the substrate and the other with (*S*)-sarin. DcPPA was modified to generate DFP by replacing the amidate group with fluoride and the two O-cyclopentyl groups with O-isopropyls. Because DcPPA binds in an unreactive orientation and because it is well-established that the substrate must be aligned for in-line attack on phosphorus[28] by Asp229, the bound substrate models were rotated ∼120° clockwise about the Ca^{2+}-coordinating O−P bond (Supporting Information, Figures S1 and S2). This modification produced a reactive orientation while also preserving Ca^{2+} coordination to the substrate. The Michaelis complex of DFPase with (*S*)-sarin was constructed by replacing the appropriate *O*-isopropyl of DFP with a methyl group.

Most of the model construction was performed with CHARMM, version c36b2.[35] Crystallographic water molecules were retained, and each system was fully solvated in an orthorhombic box of water molecules with a minimum distance of 11 Å from the protein to the nearest face of the box. Five Na^+ cations were added with the Autoionize plugin of VMD[36] to neutralize the charge of each system. Both systems contained ∼40 000 atoms. The CHARMM27 force field[37] with CMAP corrections[38] and the TIP3P water model[39] were used to describe the protein and solvent, respectively. One thousand steps of energy minimization were performed using the steepest descent algorithm. Periodic boundary conditions were applied, and the particle mesh Ewald method[40] (∼1 grid point $Å^{-3}$) was used to describe long-range electrostatic effects. The SHAKE algorithm[41] was used to constrain all bonds to hydrogen, enabling the use of a 2 fs time step. Molecular dynamics (MD) simulations were initiated by heating the systems to 300 K over 30 ps and rescaling the velocities every 1000 steps. A 5.0 kcal mol^{-1} $Å^{-2}$ harmonic restraint potential was imposed on all protein and substrate heavy atoms during the heating stages. Lastly, 0.5 ns MD simulations were performed in an NVT ensemble to equilibrate each system and to obtain initial configurations for QM/MM simulations. A 1.0 kcal mol^{-1} $Å^{-2}$ harmonic restraint potential was imposed on all protein and substrate heavy atoms during this equilibration stage.

Hybrid QM/MM Simulations. Hybrid QM/MM simulations were performed with pDynamo[42] interfaced with ORCA.[34] Representative structures were extracted near the end of the classical MD simulations and used as initial configurations. All water molecules with an oxygen atom greater than 30 Å from the phosphorus atom of the substrate were deleted to create a spherical boundary model of the system, a common approach that has been shown to yield good accuracy in investigations of enzymatic reactions.[43,44] Essentially the entire enzyme was contained within the 30 Å solvent sphere. The QM region included the DFP or (*S*)-sarin substrate, the side chains of Glu21, Asn120, Asn175, Asp229, Ser271, and Asn272, the catalytic Ca^{2+}, and two crystallographic water molecules coordinated to Ca^{2+}. Hydrogen link atoms were used to describe the QM/MM boundary, and these were automatically placed 1.0 Å away from Cβ along the Cα−Cβ bond axis for side chains in the QM region by pDynamo. The full QM regions contained 82 and 75 atoms for DFP and (*S*)-sarin, respectively. The side chain of Asp121 was also included in the QM region during the umbrella sampling (US) simulations of the hydrolysis of the phosphoenzyme intermediate with DFP substrate, for a total of 88 QM atoms. All water molecules and protein residues containing an atom greater than 20 Å from the phosphorus atom of the substrate were held fixed. For the US simulations, the QM region was described with the gradient-corrected BP86 functional[45−47] with an Ahlrichs split-valence basis set augmented with polarization and Pople diffuse functions on all N, O, F, and P atoms.[48,49] The resolution-of-the-identity approximation with the SVP/J auxiliary basis set[50] was used to reduce the computational cost of integral evaluation. In addition, Grimme atom-pairwise empirical dispersion corrections (i.e., D3)[51,52] were included. Hereafter, we refer to the combination of this DFT approach and the CHARMM molecular mechanics potential as DFT/MM.

Umbrella Sampling. Initial structures for the US simulations were obtained by performing a series of constrained geometry optimizations along a reaction coordinate defined as the mass-weighted distance difference between Oδ(Asp229)−P and P−F (referred to hereafter as the A_nD_n reaction coordinate). The US simulations were divided into 48 windows, with each having a harmonic restraint potential of 475 kcal mol^{-1} $Å^{-2}$. A 25 ps equilibration (1 fs time step) was first performed for each window with the semiempirical PM6[53]/MM hybrid potential. Each window was then further equilibrated with the DFT/MM potential for 3 ps, during which time the velocities were scaled every 100 steps until a temperature of 300 K was reached. Each window was then sampled for 20 ps in an NVT ensemble, and the reaction coordinate value was recorded at every time step. Free energy

dx.doi.org/10.1021/jp410422c | J. Phys. Chem. B 2014, 118, 4479−4489

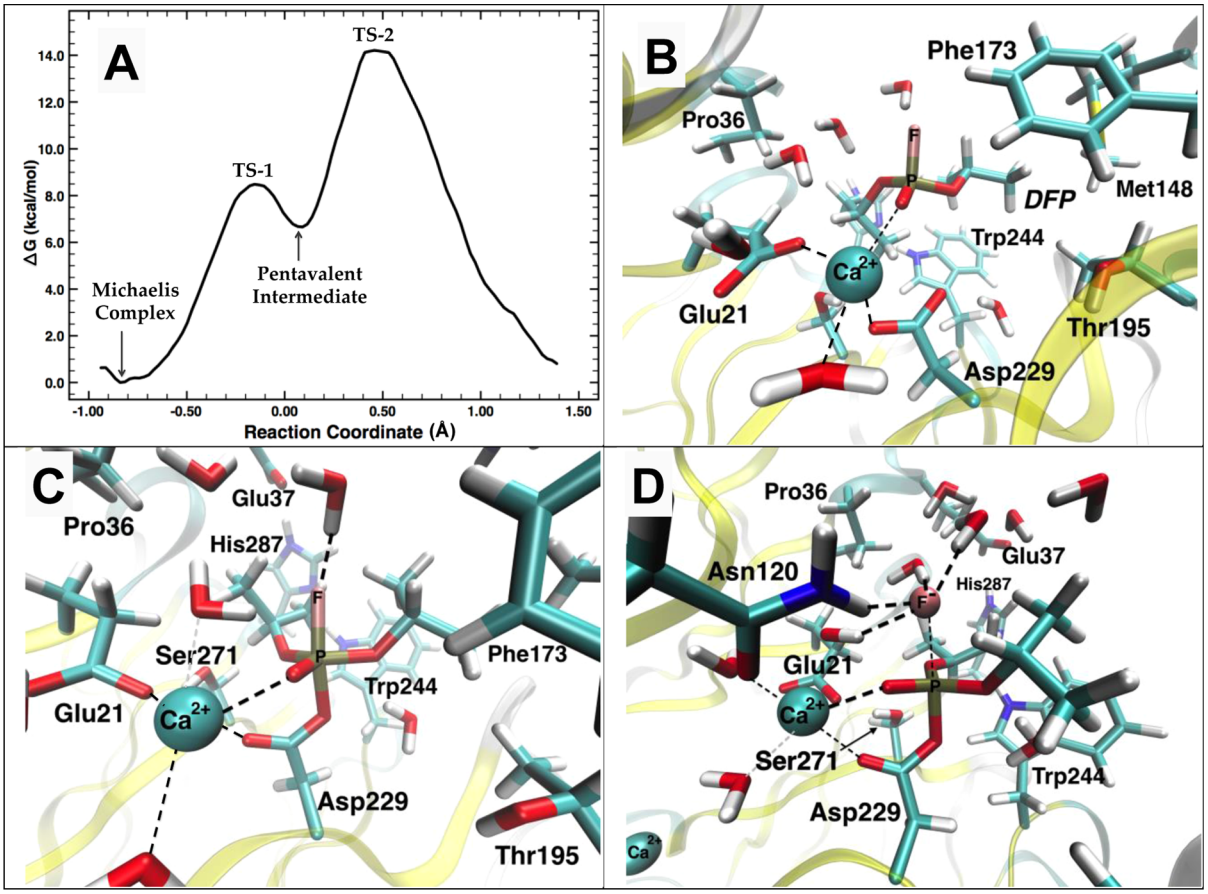

Figure 4. (A) DFT/MM US free energy profile for the $A_n + D_n$ reaction of DFPase with DFP substrate. The reaction coordinate is defined as the mass-weighted distance difference between Oδ(Asp229)−P and P−F and progresses from the Michaelis complex though the first transition state (TS-1) to the pentavalent phosphoenzyme intermediate and then through the second transition state (TS-2) to the tetrahedral phosphoenzyme intermediate at a reaction coordinate value beyond 1.4. Statistical errors range from 0.01 kcal mol^{-1} near the Michaelis complex to 0.05 kcal mol^{-1} near the tetrahedral phosphoenzyme intermediate. (B) Representative snapshot of the Michaelis complex. (C) Representative snapshot of the pentavalent phosphoenzyme intermediate. (D) Representative snapshot of the rate-limiting transition state in which fluoride dissociates from the pentavalent intermediate. Note that Ca^{2+}-coordinating residues Asn120 and Asn175 are omitted in panels B−D for clarity.

profiles were reconstructed with the weighted histogram analysis method (WHAM),[54] as implemented in the program WHAM, version 2.0.9.[55] Statistical uncertainties were estimated by performing bootstrapping analysis with 50 Monte Carlo trials.

Initial geometries for US simulations of the hydrolysis of the DFP phosphoenzyme intermediate, in which an activated water attacks Cγ of Asp229, were obtained from DFT/MM potential energy scans (see below) in which a hydroxide was formed by transferring a proton from a water molecule to Asp121. This water molecule is coordinated to the catalytic Ca^{2+} and is in close proximity to Asp121 in the joint X-ray/neutron structure (PDB entry 3BYC).[23] The reaction coordinate for these US simulations was defined as the distance difference between Cβ(Asp229)−Oδ(Asp229) and $O_{hydroxide}$−Cβ(Asp229), and 21 US windows were used to construct the potential of mean force. The fluoride anion was removed from the tetrahedral phosphoenzyme model for the simulations of subsequent hydrolysis steps.

Potential Energy Scans. DFT/MM potential energy (PE) scans were performed to characterize proton transfer energetics in the tetrahedral phosphoenzyme intermediate. The reaction coordinate was defined as the distance difference between O_{water}−H and Oδ(Asp121)−H. Gas-phase geometry optimizations were performed for acetate−DFP and acetate−(*S*)-sarin complexes, representative of pentavalent Asp229−substrate complexes, with the BP86,[45−47] *m*PWPW91,[56] *m*PW1PW91,[56] and B3LYP[57−60] functionals and the 6-31+G(d) basis set with ORCA.[34] Vibrational frequency analyses confirmed that the resulting structures were true minima. Relaxed potential energy scans were then carried out by varying the acetate-O−P(DFP/sarin) distance from 1.85 to 3.05 Å.

RESULTS AND DISCUSSION

Nucleophilic Attack of DFP by Asp229. After classical MD equilibration and subsequent QM/MM optimization of preliminary minimum energy paths obtained with the reaction coordinate driving method, DFT/MM US simulations were carried out to determine free energy profiles for each step of the reaction. The simulations indicate that the reaction proceeds by a two-step addition−elimination ($A_n + D_n$) mechanism, passing through a pentavalent intermediate common in phosphoryl transfer reactions (Figure 4).[28] A shallow free energy basin is present for the Michaelis complex (reaction coordinate ∼ −0.8 Å, see the Methods section). In the Michaelis complex, the phosphoryl oxygen of DFP and the catalytic Ca^{2+} are in close contact (∼2.6 Å) and remain in similar proximity throughout all US simulations. The *pro-S O*-isopropyl group of DFP forms

dx.doi.org/10.1021/jp410422c | J. Phys. Chem. B 2014, 118, 4479−4489

contacts with a DFPase surface comprising the side chain of Arg146 and the hydrophobic side chains of Met148, Phe173, and Thr195, whereas the opposite face of this group is exposed to solvent. The *pro-R O*-isopropyl group of DFP forms contacts with Glu21, Trp244, Ser271, and His287. The *pro-R* group has less contact with water because of shielding by the other *O*-isopropyl group. The fluorine of DFP is hydrogen-bonded to one water molecule and lacks any direct interactions with the enzyme in the Michaelis complex.

The computed free energy barrier for the nucleophilic addition step to form a metastable pentavalent species is 8.5 kcal mol^{-1}, and this step is endergonic by 6.7 kcal mol^{-1} (Figure 4). At TS-I, an additional water−F(DFP) hydrogen bond is formed that is not present earlier in the reaction. This water molecule is only weakly associated with the catalytic Ca^{2+}, with an average oxygen−Ca^{2+} distance of 3.75 Å (Figure 4), but forms a hydrogen bond with the side chain of Asn120. The pentavalent intermediate differs from TS-1 primarily in that the water molecule that was weakly coordinated to Ca^{2+} and hydrogen-bonded to the fluorine of DFP is now more strongly coordinated to Ca^{2+}, with an average oxygen−Ca^{2+} distance of 2.25 Å. A hydrogen bond between one of the amide hydrogens of the Asn175 side chain and the phosphoryl oxygen of the substrate also forms and remains intact for the remainder of the simulations.

The free energy barrier for the fluoride elimination step relative to the pentavalent intermediate with DFP substrate was computed to be 7.5 kcal mol^{-1}, yielding an overall free energy barrier of 14.2 kcal mol^{-1}. Fluoride elimination was found to proceed through a late transition state (Figure 4), in agreement with a Brønsted analysis of PON1 with paraoxon analogues as substrates.[18] At the transition state, with P−F separations averaging ∼2.3 Å, these two centers are not yet solvent-separated and maintain a direct path for recombination. The transition-state structures for fluoride elimination reveal an additional water molecule interacting with the departing fluoride. Asn120 has switched from hydrogen bonding to fluorine through a water molecule to a direct hydrogen bond, which is retained for the rest of the simulations up through the formation of the tetrahedral phosphoenzyme species. To clarify further, the fluorine of DFP has four hydrogen-bonding partners at TS-2, with three water molecules and the side chain of Asn120 all serving as donors. The underlying physical basis of this late transition state stems partly from the requirement of the departing fluoride leaving group to reach a favorable solvation environment for the free energy to reach a minimum. It is also worth noting that the water molecules partially solvating the nascent fluoride at TS-2 are adjacent to hydrophobic surfaces.

As a result, the overall reaction free energy for the reaction is less certain. Even when the A_nD_n reaction coordinate corresponded to the tetrahedral phosphoacyl enzyme intermediate (i.e., with an average P−F distance of ∼4 Å), no free energy minimum was found for the range of reaction coordinate values considered (Figure 4). A reaction occurring at or near the solvent-exposed surface of an enzyme with a product or leaving group approaching bulk solvent would not be expected to show a free energy minimum for the product state until that species is completely solvated, as has been shown in similar studies.[61] In addition, whether a free energy minimum is located at larger P−F separations is of minimal concern here because the aim of our study is to identify the factors that contribute to the overall free energy barrier. Thus, our conclusions are not affected by neglecting to identify a free energy minimum for this step.

Hydrolysis of the Phosphoenzyme Intermediate. The last step of the catalytic cycle for OP hydrolysis by DFPase has not been characterized conclusively by experiments because it is not rate limiting. Nevertheless, DFT/MM simulations suggest a possible mechanism in which a water molecule coordinated to Ca^{2+} performs a nucleophilic attack on the tetrahedral intermediate. In the joint X-ray/neutron structure of DFPase[21] and in the present simulations, a water molecule is coordinated to the catalytic Ca^{2+} and is also hydrogen-bonded to the side chain of Asp121. DFT/MM PE scans indicate that in both the Michaelis complex and in the pentavalent intermediate, this water molecule and Asp121 are in strong hydrogen-bonding contact (hydrogen-acceptor distance = 1.49 Å, donor−hydrogen-acceptor angle = 172°) in the minimum energy structures (Supporting Information, Figure S4). This geometry is consistent with the assignment of two protons on this water molecule from neutron diffraction.[21]

One of the main differences between the Michaelis complex, the pentavalent phosphoenzyme intermediate, and the tetrahedral phosphoacyl enzyme intermediate is in the coordination to the catalytic Ca^{2+} ion. Progressing from the Michaelis complex to the pentavalent intermediate, the oxygens of Asn120, the phosphoryl oxygen of DFP, and the water molecule that is hydrogen-bonded to Asp121 move closer to the catalytic Ca^{2+}, whereas the other side chains move further away. In the phosphoacyl enzyme intermediate, coordination of protein side chains to the catalytic Ca^{2+} becomes much "looser" than in the Michaelis complex. In the phosphoacyl enzyme intermediate, all oxygen−Ca^{2+} distances are longer than in the Michaelis complex and the pentavalent intermediate except for those involving the two coordinating water molecules (Supporting Information, Figure S3). Interestingly, by taking a representative tetrahedral phosphoenzyme intermediate snapshot from the US simulations and including Asp121 in the QM region, we found that a proton on the water molecule was transferred spontaneously to Asp121 (Supporting Information, Figures S3 and S4).

DFT/MM US simulations of the hydrolysis of the tetrahedral phosphoenzyme intermediate indicate that the reaction has a barrier of only 1.3 kcal mol^{-1} and is endergonic by 6.9 kcal mol^{-1} (Figure 5). The small free energy barrier is consistent with experiments showing that this step is not rate limiting.[14] As hydroxide attacks the phosphoacyl enzyme intermediate, the geometry around Cγ becomes tetrahedral and the Cγ−Oδ bond begins to break as the geometry around Cγ becomes planar. During the reaction, a hydrogen bond forms between the hydroxyl group of Ser271 and the remaining Oδ(Asp229). The distance between the phosphoryl oxygen and Ca^{2+} decreases, consistent with the computed increase in partial charge on the phosphoryl oxygen as the reaction proceeds.

The experimentally determined free energy barrier, obtained from k_{cat} with transition state theory, is 14.3 kcal mol^{-1}.[15] Our simulations yield an overall reaction free energy of 14.2 kcal mol^{-1} and are consistent with other available experimental kinetics and mutagenesis data, suggesting that the computationally determined mechanism is reasonable. The mechanism for DFPase-catalyzed inactivation of DFP was found to proceed through the nucleophilic attack by Asp229 on the phosphorus center of DFP to form a transient pentavalent intermediate followed by P−F dissociation to yield a covalent phosphoacyl intermediate in the rate-limiting step. Attack on Cγ of Asp229

dx.doi.org/10.1021/jp410422c | J. Phys. Chem. B 2014, 118, 4479−4489

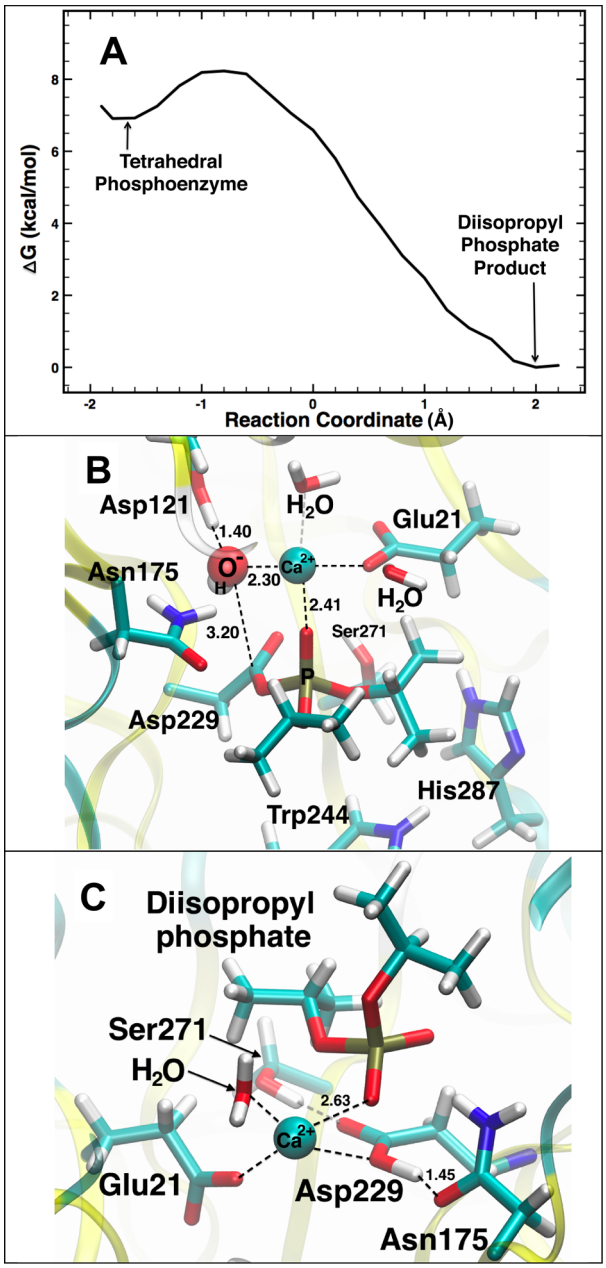

Figure 5. (A) DFT/MM US free energy profile for the nucleophilic attack of an activated water on the phosphoenzyme intermediate. The statistical error ranged from 0.01 to 0.04 kcal mol^{-1}. (B) Snapshot showing the interactions that stabilize hydroxide, which is separated from Cδ of Asp229 by 3.1 Å. (C) Enzyme-bound phosphoenzyme hydrolysis product (diisopropyl phosphate). Note that Ca^{2+}-coordinating residue Asn120 is omitted in panels B and C for clarity.

in the phosphoacyl intermediate by an activated water molecule then yields diisopropylphosphate to complete the catalytic cycle.

Hydrolysis of (*S*)-Sarin. The k_{cat}/K_m value for DFPase with (*S*)-sarin was determined to be 4.2×10^4 M^{-1} s^{-1},[15] but k_{cat} and K_m were not determined independently of each other. However, assuming that both (*S*)-sarin and DFP have similar binding affinities to DFPase, the free energy barrier derived from k_{cat} for (*S*)-sarin hydrolysis would be expected to be similar to that of DFP. Surprisingly, the computed free energy barrier for (*S*)-sarin hydrolysis by the same mechanism as DFP was significantly higher. For (*S*)-sarin, the pentavalent intermediate is completely absent and the overall free energy barrier is >14 kcal mol^{-1} higher than for DFP, at 28.6 kcal mol^{-1} (Figure 6). As is the case for DFP, the transition state for the reaction is very late, with an Oδ(Asp229)−P distance of ∼1.75 Å and a P−F distance of ∼2.4 Å. The formation of a pentavalent species with Asp229−(*S*)-sarin requires ∼16 kcal mol^{-1} more than the analogous species in DFP. Progressing from this point in the reaction coordinate (RC ∼ 0.10 Å) to the TS requires an additional 5−6 kcal mol^{-1} for (*S*)-sarin compared to 7.6 kcal mol^{-1} for DFP. Thus, the major difference between these reactions is the energetic cost of forming a pentavalent enzyme−substrate species. The computed high free energy barrier for (*S*)-sarin hydrolysis by this pathway is clearly inconsistent with experimental kinetics data, as DFPase hydrolyzes (*S*)-sarin almost as efficiently as it does DFP (k_{cat}/K_m = 4.2×10^4 versus 5.6×10^4 M^{-1} s^{-1}).[15] Therefore, the present findings indicate that the hydrolysis mechanism for (*S*)-sarin is very likely to be different from that of DFP.

In the Michaelis complex, one water molecule is hydrogen-bonded to the fluorine of sarin, and one of the amide hydrogens from the side chain of Asn120 also makes frequent hydrogen-bonding contacts with fluorine. As observed in the DFPase:DFP simulations, the phosphoryl oxygen of (*S*)-sarin remains in close contact (∼2.6 Å) with the catalytic Ca^{2+} throughout the US simulations. One major difference between the DFP and (*S*)-sarin Michaelis complexes is that with (*S*)-sarin Oδ from Asp229 is hydrogen-bonded to two water molecules. One of these water molecules is also positioned to perform an in-line nucleophilic attack on phosphorus of DFP (Figure 7). This water molecule is displaced during the formation of the pentavalent structure of DFPase:(*S*)-sarin, but the other remains stably bound in the active site. The hydrogen-bonding partners with fluorine remain the same as in the Michaelis complex. At the transition state, an additional water molecule hydrogen bonds to the departing fluoride. The water molecule interacting with Oδ of Asp229 becomes hydrogen bonded to *O*-isopropyl oxygen late in the reaction. In the final US window, the fluoride is hydrogen-bonded to four water molecules. As with the departing fluoride of DFP, the water molecules that are hydrogen-bonded to the fluoride of (*S*)-sarin are adjacent to a hydrophobic surface of the enzyme and are not in a favorable solvation environment. The hydrogen bond between Asn120 and the fluoride has been replaced by another hydrogen bond between Asn120 and the phosphoryl oxygen of the phosphoenzyme intermediate.

To investigate the underlying reactivity of Asp229 as a nucleophile reacting with DFP and (*S*)-sarin, we performed gas-phase geometry optimizations and PE scans with the BP86, B3LYP, *m*PWPW91, and *m*PW1PW91 density functionals and the 6-31+G(d) basis set on isolated models of Asp229−substrate adducts, with Asp229 being represented by acetate. Stable pentavalent structures were identified for the acetate−DFP complex with all four functionals (Figure 8). However, none yielded a stable pentavalent structure for the acetate−sarin complex. Electron-donating substituents at equatorial positions are known to destabilize pentavalent phosphorus species.[62] DFP is better able to stabilize the negative charge from the carboxylate nucleophile with its two *O*-isopropyl substituents than (*S*)-sarin, which contains one *O*-isopropyl and one methyl group. From the DFT/MM simulations, the larger partial negative charge on the nucleophilic Asp229−Oδ in (*S*)-sarin versus DFP and the large partial negative charge on the

dx.doi.org/10.1021/jp410422c | J. Phys. Chem. B 2014, 118, 4479−4489

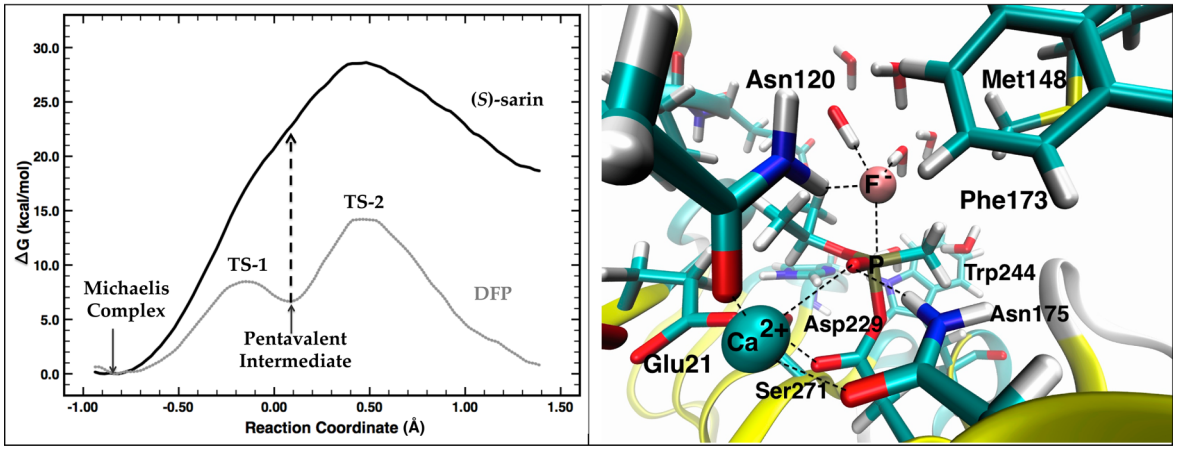

Figure 6. (Left) DFT/MM US free energy profile for the A_nD_n reaction of DFPase with (*S*)-sarin. The arrow from the DFP:DFPase pentavalent intermediate basin to the corresponding point in the DFPase:(*S*)-sarin free energy profile is shown to highlight the complete lack of this intermediate in the reaction with (*S*)-sarin. Statistical errors range from 0.01 kcal mol^{-1} near the Michaelis complex to 0.06 kcal mol^{-1} near the tetrahedral phosphoenzyme intermediate. (Right) Representative snapshot of the transition state from the DFT/MM US simulation of the DFPase:(*S*)-sarin reaction.

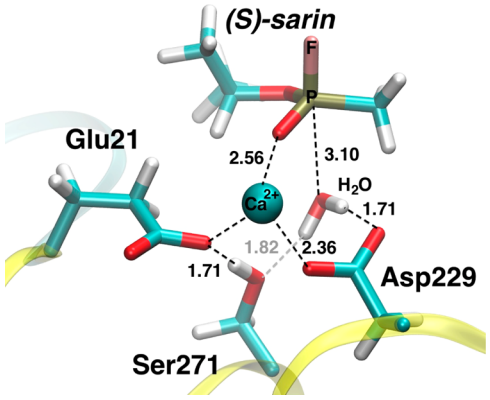

Figure 7. Snapshot from DFT/MM simulations of DFPase/(*S*)-sarin supporting a nucleophilic attack on the phosphorus center of (*S*)-sarin hydrolysis by a water molecule upon activation by proton transfer to Asp229. Selected distances shown are shown in angstroms. Ca^{2+}-coordinating residues Asn120 and Asn175 are omitted for clarity.

methyl carbon in (*S*)-sarin support the above rationale (Supporting Information, Table S1).

The physicochemical factors that lead to the vastly different free energy profiles for the two substrates stem from (1) the difference in the ability of the two substrates to accommodate the additional negative charge from the incoming Asp229 nucleophile and (2) competing interactions between the electrophilic phosphorus and water molecules with Asp229. Thus, the findings from the QM/MM simulations can be traced to differences in the electrophilicity and reactivity of the phosphorus centers in DFP and (*S*)-sarin.

Given the high calculated free energy barrier for the concerted but highly asynchronous (A_nD_n) reaction of Asp229 with (*S*)-sarin and the complete absence of a metastable pentavalent intermediate, we considered the possibility of an alternative mechanism in which Asp229 activates an ordered water molecule, which then attacks phosphorus (either in a stepwise or concerted reaction). In the first five windows of the US simulations of DFPase:(*S*)-sarin, a water molecule from the MM region is hydrogen-bonded to both Asp229 and Ser271 and is positioned between

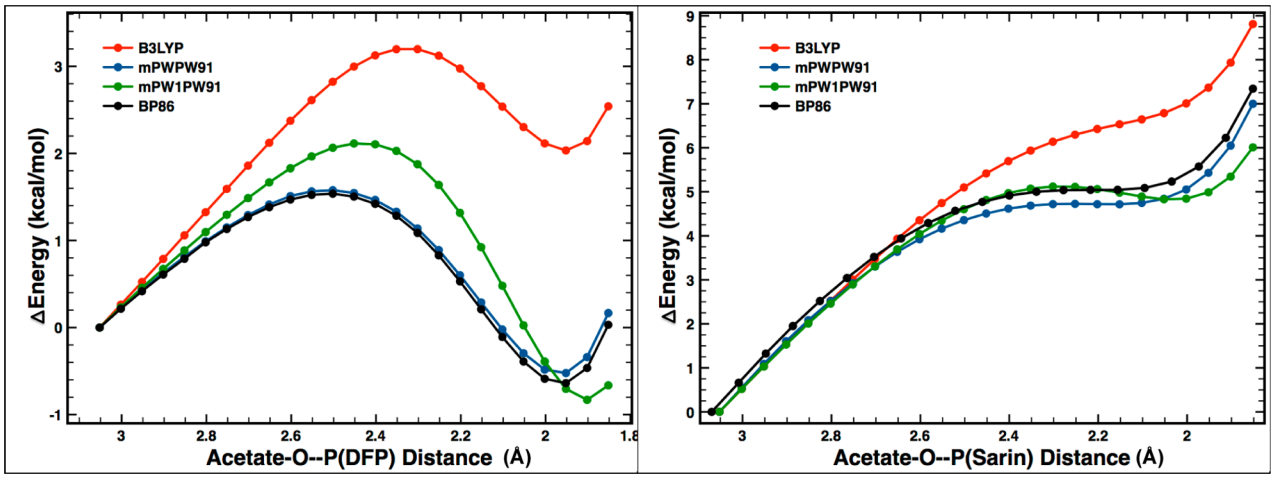

Figure 8. Gas-phase potential energy scans obtained by varying the acetate−O−P distance in (left) acetate−DFP and (right) acetate−sarin obtained with the BP86, B3LYP, *m*PWPW91, and *m*PW1PW91 functionals and the 6-31+G(d) basis set.

dx.doi.org/10.1021/jp410422c | J. Phys. Chem. B 2014, 118, 4479−4489

these residues and (*S*)-sarin (Figure 7). The catalytic Ca^{2+} is not expected to affect the nucleophilicity of this water molecule because it is ∼5 Å away in the simulations. Inclusion of this water molecule in the QM region would be expected to polarize it further through its hydrogen-bonding interactions with Asp229. Thus, it is possible that Asp229 could activate the water molecule for nucleophilic attack on the substrate rather than performing the nucleophilic attack directly. Simulating this process would require exploration of 2D free energy surfaces, the computational cost of which is prohibitive with the DFT/MM methods used here. Whereas only multiple-turnover kinetics assays with DFP substrate in $H_2{}^{18}O$ yielded an ^{18}O-labeled hydrolysis product,[14] our simulations predict that both single- and multiple-turnover assays with (*S*)-sarin should incorporate the ^{18}O label into the hydrolysis product, isopropyl methylphosphonate.

Implications for Engineering DFPase for Hydrolysis of Nerve Agents. A bioinformatics study[22] of six-bladed β-propeller enzymes that carry out nucleophilic attack placed DFPases within a subgroup consisting of SMP-30/gluconolactonase/luciferin-regenerating (SGL) enzymes, whereas the paraoxonases were placed in an arylesterase subgroup. SMP-30 is involved in L-ascorbic acid biosynthesis in nonprimate mammals but has also been investigated for its OP hydrolytic capabilities.[63] SMP-30 shares some active site residues with DFPase but has very poor activity against G-type nerve agents due, in part, to its poor substrate binding characteristics.[25] The promiscuity of enzymes bearing the six-bladed β-propeller fold is immense,[22] thus seemingly providing an excellent platform to design enzymes with alternate functions. Indeed, DFPase has even served as a scaffold to design a Diels−Alderase.[64]

On the basis of in vivo protection experiments, catalytic efficiencies (k_{cat}/K_m) ≥ 10^7 M^{-1} min^{-1} are required for effective prophylaxis against 2 × LD_{50} of G-type agents using minimal enzyme doses (≤50 mg/70 kg).[13] Through a combination of rational design and directed evolution, PON1 variants have been developed with rates of hydrolysis of G-type nerve agents that are enhanced by at least 340-fold relative to wild type. The catalytic efficiencies (k_{cat}/K_m) of the best PON1 variants with GB, GD, and GF substrates are 5 × 10^3, 1.2 × 10^4, and 2.9 × 10^5 M^{-1} s^{-1}, respectively. A similar approach combining rational design and directed evolution was used to engineer PTE variants that hydrolyze the (*S*)-enantiomers of GB, GD, and GF with k_{cat}/K_m values of 2 × 10^6, 5 × 10^5, and 8 × 10^5 M^{-1} s^{-1}, respectively. Wild-type DFPase exhibits a catalytic efficiency for (*S*)-GB (k_{cat}/K_m = 4.2 × 10^4 M^{-1} s^{-1}) that is almost 1 order of magnitude higher than the current best PON1 variant. For (*S*)-GF (k_{cat}/K_m = 1.7 × 10^4 M^{-1} s^{-1}), DFPase has 17-fold lower activity than the best PON1 variant.[15] A rationally designed quadruple mutant (Glu37Ala/Tyr144Ala/Arg146Ala/Thr195Met) of DFPase displayed reversed enantioselectivity to favor the more toxic (*S*)-enantiomers of GB and GF, simultaneously increasing the catalytic efficiencies to 2.3 × 10^5 and 4.9 × 10^5 M^{-1} s^{-1}, respectively.[15] Exchanging three bulky residues with alanines resulted in a more accessible active site, and introducing a negative design element (Thr195Met) hindered the binding of the less-toxic (*R*)-enantiomers of GB and GF.

The QM/MM simulations performed in this work have implications for engineering DFPase nerve agent bioscavengers and possibly other six-bladed β-propeller enzymes such as PON1[12] and SMP-30.[25] The simulations suggest ways to optimize enzymes for more efficient catalysis. To lower the barrier for fluoride elimination, the local environment should be sufficiently hydrophilic to allow for fluoride solvation. In DFPase, hydrophobic residues such as Met90, Met148, and Phe173 (Supporting Information, Figure S2) create an unfavorable solvation environment for the fluoride anion and may hinder the expulsion of the leaving group. Therefore, proper placement of positively charged side chains (Arg and Lys) or hydrogen-bond donors that could interact favorably with the developing negative charge on fluorine or facilitate improved solvation is a strategy worth exploring. Our simulations also show that Tyr144 is near the path of the departing fluoride anion in the rate-limiting elimination step. Tyr144 was mutated to Ala in the quadruple mutant of DFPase,[15] which presumably allows greater solvation of fluoride and lowers the free energy barrier for the rate-determining step.

Furthermore, the present simulations also provide an interpretation of the effect of the mutations reported by Goldsmith et al. in their rational and directed evolution design efforts to develop a broad-spectrum G-type nerve agent detoxifying enzyme.[12] In rePON1 variant IIG1, active site residues Thr332 and His115 were mutated to Ser and Ala, respectively, thereby creating an active site that was almost identical to that of DFPase. The second-sphere His134Arg mutation was thought to compensate for the His115Ala mutation. However, because His134 is oriented toward the active site in PON1 structures, mutating it to Arg while also changing His115 to Ala might expose the positively charged Arg side chain to the active site and place it in a position to assist in the departure of the fluoride leaving group. Recall that this reaction has a very late transition state (i.e., the developing fluoride is several angstroms from the substrate phosphorus). Thus, the favorable interactions between an exposed Arg134 and the leaving group may partially explain the large increase in catalytic efficiency seen in the PG11 variant for soman (GD) hydrolysis. Further improvement in catalytic efficiency was found upon adding the Asp136Gln mutation.[12] Asp136, like His134, is oriented toward the active site and would not interact favorably with a departing fluoride anion. Thus, its replacement could assist in lowering the barrier for the elimination reaction, although a similar mutation in DFPase would not be possible because the aspartate is located in a nonhomologous loop region.

Mechanistic interpretations for DFPase do not necessarily transfer to PON1 because their active sites differ slightly, most notably with respect to His115(PON1)/Ala74(DFPase), which enables other mechanistic possibilities to be entertained. For example, instead of a direct nucleophilic attack by Asp on the substrate, it has been proposed that a His134−His115 dyad in PON1 activates a water molecule for attack.[24] Extensive site-directed mutagenesis studies support this mechanism for the PON1-catalyzed hydrolysis of lactones, but these residues do not appear to play roles in OP hydrolase activity.[65] On the basis of MD simulations, Asp269 in PON1 has also been proposed to activate a water molecule for attack on OP substrates.[66,67]

Perhaps the most significant implication of the present findings is that replacing an electron-acceptor group (*O*-isopropyl) in the DFP substrate with an electron donor (methyl) in (*S*)-sarin is sufficient to alter the hydrolysis reaction mechanism. This result, determined with quantitatively accurate DFT/MM simulations, was unexpected given that the catalytic efficiencies for both substrates are similar. The methyl group in sarin precludes the formation of a pentavalent phosphoenzyme

dx.doi.org/10.1021/jp410422c | J. Phys. Chem. B 2014, 118, 4479−4489

intermediate, as we have shown with simple gas-phase calculations on acetate−sarin and acetate−DFP complexes. Of course, the enzyme environment can also be a significant factor in stabilizing a pentavalent phosphorus structure,[68] but the calculations indicate that the enzyme environment actually contributes further to the destabilization with (*S*)-sarin. The less bulky methyl group allows water molecules to be in closer proximity to Asp229, and the interactions of water with Asp229 are likely to be more favorable than those with phosphorus. Other nerve agents such as soman and VX also have a single methyl group bonded to phosphorus. These nerve agents may also undergo hydrolysis by DFPase and related enzymes through an alternate mechanism, although other factors will undoubtedly play a role.

The reactivity of carboxylate nucleophiles toward a given OP substrate should be considered in bioscavenger design efforts. However, it remains to be seen whether nucleophilic attack by Asp229 or water/hydroxide is preferable. Nevertheless, insight gained from mechanistic simulation studies can serve as a guide for rational design and as a starting point for further optimization and refinement through directed evolution.

■ ASSOCIATED CONTENT

Supporting Information

Details on the construction of the initial simulation models, active site structures of representative DFPase:DFP intermediates, potential energy profiles for proton transfer between Asp121 and an active site water molecule, and Löwdin charges of pentavalent species. This material is available free of charge via the Internet at http://pubs.acs.org.

■ AUTHOR INFORMATION

Corresponding Authors

*(T.W.) Tel.: (865) 241-3063; E-mail: wymoretw@ornl.gov.
*(J.M.P.) Tel.: (865) 574-9259; E-mail: parksjm@ornl.gov.

Notes

The authors declare no competing financial interest.

■ ACKNOWLEDGMENTS

This research was sponsored by the Laboratory Directed Research and Development Program at Oak Ridge National Laboratory, which is managed by UT-Battelle, LLC, for the U.S. Department of Energy (DOE). This work was also supported by DOE/NNSA under contract DE-AC05-00OR22752 and by the National Institutes of Health (1P41 GM103712-01).

■ ABBREVIATIONS

DFP, diisopropyl fluorophosphate; DFPase, diisopropyl fluorophosphatase; sarin, GB, isopropyl methylphosphonofluoridate

■ REFERENCES

(1) Worek, F.; Thiermann, H.; Szinicz, L.; Eyer, P. Kinetic analysis of interactions between human acetylcholinesterase, structurally different organophosphorus compounds and oximes. *Biochem. Pharmacol.* **2004**, *68*, 2237−2248.

(2) Hörnberg, A.; Artursson, E.; Wärme, R.; Pang, Y.-P.; Ekström, F. Crystal structures of oxime-bound fenamiphos-acetylcholinesterases: Reactivation involving flipping of the His447 ring to form a reactive Glu334−His447−oxime triad. *Biochem. Pharmacol.* **2010**, *79*, 507−515.

(3) Mercey, G.; Verdelet, T.; Saint-Andre, G.; Gillon, E.; Wagner, A.; Baati, R.; Jean, L.; Nachon, F.; Renard, P. Y. First efficient uncharged reactivators for the dephosphylation of poisoned human acetylcholinesterase. *Chem. Commun.* **2011**, *47*, 5295−5297.

(4) Kovach, I. M. Stereochemistry and secondary reactions in the irreversible inhibition of serine hydrolases by organophosphorus compounds. *J. Phys. Org. Chem.* **2004**, *17*, 602−614.

(5) Michel, H. O.; Hackley, B. E.; Berkowitz, L.; List, G.; Hackley, E. B.; Gillilan, W.; Pankau, M. Ageing and dealkylation of soman (pinacolylmethylphosphono-fluoridate)-inactivated eel cholinesterase. *Arch. Biochem. Biophys.* **1967**, *121*, 29−34.

(6) Masson, P. Evolution of and perspectives on therapeutic approaches to nerve agent poisoning. *Toxicol. Lett.* **2011**, *206*, 5−13.

(7) Raushel, F. M. Chemical biology: Catalytic detoxification. *Nature* **2011**, *469*, 310−311.

(8) Nachon, F.; Brazzolotto, X.; Trovaslet, M.; Masson, P. Progress in the development of enzyme-based nerve agent bioscavengers. *Chem.−Biol. Interact.* **2013**, *206*, 536−544.

(9) Tsai, P. C.; Fox, N.; Bigley, A. N.; Harvey, S. P.; Barondeau, D. P.; Raushel, F. M. Enzymes for the homeland defense: Optimizing phosphotriesterase for the hydrolysis of organophosphate nerve agents. *Biochemistry* **2012**, *51*, 6463−6475.

(10) Cherny, I.; Greisen, P., Jr.; Ashani, Y.; Khare, S. D.; Oberdorfer, G.; Leader, H.; Baker, D.; Tawfik, D. S. Engineering V-type nerve agents detoxifying enzymes using computationally focused libraries. *ACS Chem. Biol.* **2013**, *8*, 2394−2403.

(11) Bigley, A. N.; Raushel, F. M. Catalytic mechanisms for phosphotriesterases. *Biochim. Biophys. Acta* **2013**, *1834*, 443−453.

(12) Goldsmith, M.; Ashani, Y.; Simo, Y.; Ben-David, M.; Leader, H.; Silman, I.; Sussman, J. L.; Tawfik, D. S. Evolved stereoselective hydrolases for broad-spectrum G-type nerve agent detoxification. *Chem. Biol.* **2012**, *19*, 456−466.

(13) Gupta, R. D.; Goldsmith, M.; Ashani, Y.; Simo, Y.; Mullokandov, G.; Bar, H.; Ben-David, M.; Leader, H.; Margalit, R.; Silman, I.; et al. Directed evolution of hydrolases for prevention of G-type nerve agent intoxication. *Nat. Chem. Biol.* **2011**, *7*, 120−125.

(14) Blum, M.-M.; Löhr, F.; Richardt, A.; Rüterjans, H.; Chen, J. C.-H. Binding of a designed substrate analogue to diisopropyl fluorophosphatase: Implications for the phosphotriesterase mechanism. *J. Am. Chem. Soc.* **2006**, *128*, 12750−12757.

(15) Melzer, M.; Chen, J. C.-H.; Heidenreich, A.; Gäb, J.; Koller, M.; Kehe, K.; Blum, M.-M. Reversed enantioselectivity of diisopropyl fluorophosphatase against organophosphorus nerve agents by rational design. *J. Am. Chem. Soc.* **2009**, *131*, 17226−17232.

(16) Hartleib, J.; Ruterjans, H. Insights into the reaction mechanism of the diisopropyl fluorophosphatase from *Loligo vulgaris* by means of kinetic studies, chemical modification and site-directed mutagenesis. *Biochim. Biophys. Acta* **2001**, *1546*, 312−324.

(17) Katsemi, V.; Lucke, C.; Koepke, J.; Lohr, F.; Maurer, S.; Fritzsch, G.; Ruterjans, H. Mutational and structural studies of the diisopropylfluorophosphatase from *Loligo vulgaris* shed new light on the catalytic mechanism of the enzyme. *Biochemistry* **2005**, *44*, 9022−9033.

(18) Khersonsky, O.; Tawfik, D. S. Structure−reactivity studies of serum paraoxonase PON1 suggest that its native activity is lactonase. *Biochemistry* **2005**, *44*, 6371−6382.

(19) Koepke, J.; Scharff, E. I.; Lucke, C.; Ruterjans, H.; Fritzsch, G. Statistical analysis of crystallographic data obtained from squid ganglion DFPase at 0.85 A resolution. *Acta Crystallogr., Sect. D: Biol. Crystallogr.* **2003**, *59*, 1744−1754.

(20) Scharff, E. I.; Koepke, J.; Fritzsch, G.; Lucke, C.; Ruterjans, H. Crystal structure of diisopropylfluorophosphatase from *Loligo vulgaris*. *Structure* **2001**, *9*, 493−502.

(21) Blum, M.-M.; Mustyakimov, M.; Rüterjans, H.; Kehe, K.; Schoenborn, B. P.; Langan, P.; Chen, J. C.-H. Rapid determination of hydrogen positions and protonation states of diisopropyl fluorophosphatase by joint neutron and X-ray diffraction refinement. *Proc. Natl. Acad. Sci. U.S.A.* **2009**, *106*, 713−718.

(22) Hicks, M. A.; Barber, A. E.; Giddings, L.-A.; Caldwell, J.; O'connor, S. E.; Babbitt, P. C. The evolution of function in strictosidine synthase-like proteins. *Proteins: Struct., Funct., Bioinf.* **2011**, *79*, 3082−3098.
(23) Chen, J. C. H.; Mustyakimov, M.; Schoenborn, B. P.; Langan, P.; Blum, M. M. Neutron structure and mechanistic studies of diisopropyl fluorophosphatase (DFPase). *Acta Crystallogr., Sect. D: Biol. Crystallogr.* **2010**, *66*, 1131−1138.
(24) Harel, M.; Aharoni, A.; Gaidukov, L.; Brumshtein, B.; Khersonsky, O.; Meged, R.; Dvir, H.; Ravelli, R. B. G.; Mccarthy, A.; Toker, L.; et al. Structure and evolution of the serum paraoxonase family of detoxifying and anti-atherosclerotic enzymes. *Nat. Struct. Mol. Biol.* **2004**, *11*, 412−419.
(25) Belinskaya, T.; Pattabiraman, N.; Ditargiani, R.; Choi, M.; Saxena, A. Differences in amino acid residues in the binding pockets dictate substrate specificities of mouse senescence marker protein-30, human paraoxonase 1, and squid diisopropylfluorophosphatase. *Biochim. Biophys. Acta* **2012**, *1824*, 701−710.
(26) Elias, M.; Liebschner, D.; Koepke, J.; Lecomte, C.; Guillot, B.; Jelsch, C.; Chabriere, E. Hydrogen atoms in protein structures: High-resolution X-ray diffraction structure of the DFPase. *BMC Res. Notes* **2013**, *6*, 308-1−308-7.
(27) Guthrie, R. D.; Jencks, W. P. IUPAC recommendations for the representation of reaction mechanisms. *Acc. Chem. Res.* **1989**, *22*, 343−349.
(28) Cleland, W. W.; Hengge, A. C. Enzymatic mechanisms of phosphate and sulfate transfer. *Chem. Rev.* **2006**, *106*, 3252−3278.
(29) Warshel, A.; Levitt, M. Theoretical studies of enzymic reactions: dielectric, electrostatic and steric stabilization of the carbonium ion in the reaction of lysozyme. *J. Mol. Biol.* **1976**, *103*, 227−249.
(30) Gao, J.; Ma, S.; Major, D. T.; Nam, K.; Pu, J.; Truhlar, D. G. Mechanisms and free energies of enzymatic reactions. *Chem. Rev.* **2006**, *106*, 3188−3209.
(31) Senn, H. M.; Thiel, W. QM/MM methods for biomolecular systems. *Angew. Chem., Int. Ed.* **2009**, *48*, 1198−1229.
(32) Vanommeslaeghe, K.; MacKerell, A. D., Jr. Automation of the CHARMM general force field (CGenFF) I: Bond perception and atom typing. *J. Chem. Inf. Model.* **2012**, *52*, 3144−3154.
(33) Vanommeslaeghe, K.; Raman, E. P.; MacKerell, A. D., Jr. Automation of the CHARMM general force field (CGenFF) II: Assignment of bonded parameters and partial atomic charges. *J. Chem. Inf. Model.* **2012**, *52*, 3155−3168.
(34) Neese, F. The ORCA program system. *Wiley Interdiscip. Rev.: Comput. Mol. Sci.* **2012**, *2*, 73−78.
(35) Brooks, B. R.; Brooks, C. L.; Mackerell, A. D.; Nilsson, L.; Petrella, R. J.; Roux, B.; Won, Y.; Archontis, G.; Bartels, C.; Boresch, S.; et al. CHARMM: The biomolecular simulation program. *J. Comput. Chem.* **2009**, *30*, 1545−1614.
(36) Humphrey, W.; Dalke, A.; Schulten, K. VMD − Visual Molecular Dynamics. *J. Mol. Graphics* **1996**, *14*, 33−38.
(37) Mackerell, A. D. Empirical force fields for biological macromolecules: Overview and issues. *J. Comput. Chem.* **2004**, *25*, 1584−1604.
(38) MacKerell, A. D.; Feig, M.; Brooks, C. L. Improved treatment of the protein backbone in empirical force fields. *J. Am. Chem. Soc.* **2004**, *126*, 698−699.
(39) Jorgensen, W. L.; Chandrasekhar, J.; Madura, J. D.; Impey, R. W.; Klein, M. L. Comparison of simple potential functions for simulating liquid water. *J. Chem. Phys.* **1983**, *79*, 926−935.
(40) Darden, T.; York, D.; Pedersen, L. Particle mesh Ewald - An N Log(N) method for Ewald sums in large systems. *J. Chem. Phys.* **1993**, *98*, 10089−10092.
(41) Ryckaert, J. P.; Ciccotti, G.; Berendsen, H. J. C. Numerical integration of Cartesian equations of motion of a system with constraints − Molecular dynamics of N-alkanes. *J. Comput. Phys.* **1977**, *23*, 327−341.
(42) Field, M. The pDynamo program for molecular simulations using hybrid quantum chemical and molecular mechanical potentials. *J. Chem. Theory Comput.* **2008**, *4*, 1151−1161.
(43) Wu, R.; Wang, S.; Zhou, N.; Cao, Z.; Zhang, Y. A proton-shuttle reaction mechanism for histone deacetylase 8 and the catalytic role of metal ions. *J. Am. Chem. Soc.* **2010**, *132*, 9471−9479.
(44) Rosta, E.; Nowotny, M.; Yang, W.; Hummer, G. Catalytic mechanism of RNA backbone cleavage by ribonuclease H from quantum mechanics/molecular mechanics simulations. *J. Am. Chem. Soc.* **2011**, *133*, 8934−8941.
(45) Perdew, J. P.; Zunger, A. Self-interaction correction to density-functional approximations for many-electron systems. *Phys. Rev. B* **1981**, *23*, 5048−5079.
(46) Perdew, J. P. Density-functional approximation for the correlation energy of the inhomogeneous electron gas. *Phys. Rev. B* **1986**, *33*, 8822−8824.
(47) Becke, A. D. Density-functional exchange-energy approximation with correct asymptotic behavior. *Phys. Rev. A* **1988**, *38*, 3098−3100.
(48) Krishnan, R.; Binkley, J. S.; Seeger, R.; Pople, J. A. Self-consistent molecular-orbital methods. 20. Basis set for correlated wave-functions. *J. Chem. Phys.* **1980**, *72*, 650−654.
(49) Mclean, A. D.; Chandler, G. S. Contracted Gaussian-basis sets for molecular calculations. 1. 2nd row atoms, Z=11−18. *J. Chem. Phys.* **1980**, *72*, 5639−5648.
(50) Eichkorn, K.; Weigend, F.; Treutler, O.; Ahlrichs, R. Auxiliary basis sets for main row atoms and transition metals and their use to approximate Coulomb potentials. *Theor. Chem. Acc.* **1997**, *97*, 119−124.
(51) Grimme, S.; Ehrlich, S.; Goerigk, L. Effect of the damping function in dispersion corrected density functional theory. *J. Comput. Chem.* **2011**, *32*, 1456−1465.
(52) Grimme, S.; Antony, J.; Ehrlich, S.; Krieg, H. A consistent and accurate ab initio parametrization of density functional dispersion correction (DFT-D) for the 94 elements H-Pu. *J. Chem. Phys.* **2010**, *132*, 154104-1−154104-19.
(53) Stewart, J. J. P. Optimization of parameters for semiempirical methods V: Modification of NDDO approximations and application to 70 elements. *J. Mol. Model.* **2007**, *13*, 1173−1213.
(54) Kumar, S.; Rosenberg, J. M.; Bouzida, D.; Swendsen, R. H.; Kollman, P. A. Multidimensional free-energy calculations using the weighted histogram analysis method. *J. Comput. Chem.* **1995**, *16*, 1339−1350.
(55) Grossfield, A. WHAM: The weighted histogram analysis method, version 2.09. http://membrane.urmc.rochester.edu/content/wham.
(56) Adamo, C.; Barone, V. Exchange functionals with improved long-range behavior and adiabatic connection methods without adjustable parameters: The mPW and mPW1PW models. *J. Chem. Phys.* **1998**, *108*, 664−675.
(57) Becke, A. D. Density-functional thermochemistry 0.3. The role of exact exchange. *J. Chem. Phys.* **1993**, *98*, 5648−5652.
(58) Lee, C. T.; Yang, W. T.; Parr, R. G. Development of the Colle−Salvetti correlation-energy formula into a functional of the electron-density. *Phys. Rev. B* **1988**, *37*, 785−789.
(59) Vosko, S. H.; Wilk, L.; Nusair, M. Accurate spin-dependent electron liquid correlation energies for local spin-density calculations − a critical analysis. *Can. J. Phys.* **1980**, *58*, 1200−1211.
(60) Stephens, P. J.; Devlin, F. J.; Chabalowski, C. F.; Frisch, M. J. Ab-initio calculation of vibrational absorption and circular-dichroism spectra using density-functional force-fields. *J. Phys. Chem.* **1994**, *98*, 11623−11627.
(61) Lopez-Canut, V.; Ruiz-Pernia, J. J.; Castillo, R.; Moliner, V.; Tunon, I. Hydrolysis of phosphotriesters: A theoretical analysis of the enzymatic and solution mechanisms. *Chem.—Eur. J.* **2012**, *18*, 9612−9621.
(62) Marcos, E.; Anglada, J. M.; Crehuet, R. Description of pentacoordinated phosphorus under an external electric field: Which basis sets and semi-empirical methods are needed? *Phys. Chem. Chem. Phys.* **2008**, *10*, 2442−2450.
(63) Kondo, Y.; Inai, Y.; Sato, Y.; Handa, S.; Kubo, S.; Shimokado, K.; Goto, S.; Nishikimi, M.; Maruyama, N.; Ishigami, A. Senescence marker protein 30 functions as gluconolactonase in L-ascorbic acid

biosynthesis, and its knockout mice are prone to scurvy. *Proc. Natl. Acad. Sci. U.S.A.* **2006**, *103*, 5723−5728.
(64) Siegel, J. B.; Zanghellini, A.; Lovick, H. M.; Kiss, G.; Lambert, A. R.; St. Clair, J. L.; Gallaher, J. L.; Hilvert, D.; Gelb, M. H.; Stoddard, B. L.; et al. Computational design of an enzyme catalyst for a stereoselective bimolecular Diels−Alder reaction. *Science* **2010**, *329*, 309−313.
(65) Khersonsky, O.; Tawfik, D. S. The histidine 115-histidine 134 dyad mediates the lactonase activity of mammalian serum paraoxonases. *J. Biol. Chem.* **2006**, *281*, 7649−7656.
(66) Hu, X.; Jiang, X.; Lenz, D. E.; Cerasoli, D. M.; Wallqvist, A. In silico analyses of substrate interactions with human serum paraoxonase 1. *Proteins: Struct., Funct., Bioinf.* **2009**, *75*, 486−498.
(67) Muthukrishnan, S.; Shete, V. S.; Sanan, T. T.; Vyas, S.; Oottikkal, S.; Porter, L. M.; Magliery, T. J.; Hadad, C. M. Mechanistic insights into the hydrolysis of organophosphorus compounds by paraoxonase-1: Exploring the limits of substrate tolerance in a promiscuous enzyme. *J. Phys. Org. Chem.* **2012**, *25*, 1247−1260.
(68) Marcos, E.; Crehuet, R.; Anglada, J. M. Inductive and external electric field effects in pentacoordinated phosphorus compounds. *J. Chem. Theory Comput.* **2008**, *4*, 49−63.